

The mechanical tension of biomembranes can be measured by super resolution (STED) microscopy of force-induced nanotubes

Debjit Roy^{1,2}, Jan Steinkühler¹, Ziliang Zhao¹, Reinhard Lipowsky¹ and Rumiana Dimova^{1*}

¹Department of Theory and Bio-Systems, Max Planck Institute of Colloids and Interfaces, Science Park Golm, 14424 Potsdam, Germany

²Present address: Department of Biochemistry and Molecular Biophysics, Washington University School of Medicine, St. Louis, Missouri 63110, USA

* Address correspondence to Rumiana.Dimova@mpikg.mpg.de

S1 Vesicle preparation

Giant unilamellar vesicles (GUVs) were prepared using the electroformation method¹⁻². The vesicles were prepared from 1-palmitoyl-2-oleoyl-sn-glycero-3-phosphatidylcholine (POPC) (Avanti Polar Lipids) dissolved in chloroform at concentration of 2 mM. To ensure adhesion between GUVs and streptavidin coated beads, the membrane was doped with 0.1 mol% of biotinyl cap phosphatidylethanolamine (PE) (Avanti Polar Lipids). The membrane was stained with the fluorescent dye 0.5 mol% ATTO 647N (ATTO Tech). 4 μ l of the lipid solution was spread uniformly on the conductive sides of two indium tin oxide coated glass plates, and dried under vacuum for one hour to evaporate the chloroform. The two glass plates were assembled using a 2 mm thick Teflon spacer to form a closed chamber of volume \sim 1700 μ l. 100 mOsm/kg sucrose solution was used to fill the chamber as growing medium. The solution osmolarity as well as that of the external vesicle solution was adjusted with freezing point osmometer Osmomat 3000 (Gonotec). A sinusoidal AC electric field at 10 Hz frequency with RMS amplitude 0.75 V, measured at the ITO coated glass plates, was applied for the electrosweeling process for 2 hours. The grown GUVs were harvested afterwards and transferred to glass containers for further investigations. All experiments were performed at room temperature (\sim 22°C).

S2 Fluctuation analysis

The bending rigidity of a GUV can be obtained by analyzing the thermal fluctuations of the equatorial plane contour. Following a previously published protocol³, for each vesicle, 10000 snapshots were collected at an acquisition speed of 50 frames per second with 200 μ s exposure time using a fast digital camera HG-100K (Redlake Inc., USA). The vesicles were recorded at their focal on inverted microscope Axiovert 135. The measurements were done under the same buffer condition at which the tube pulling experiments were performed. From the shape fluctuation analysis of five GUVs, the average bending rigidity is found to be (23 ± 2) $k_B T$, see Table S1 for data on the individual measurements.

Table S1. Bending rigidity obtained from fluctuation analysis. The numbers in the brackets indicate the measurement error.

GUV Number	Bending Rigidity, $k_B T$
1	23 (2)
2	25 (3)
3	21 (3)
4	22 (2)
5	25 (2)
Average Value	23 ± 2

S3 Experimental setup

The experimental set-up consists of three parts: micropipette system to hold and aspirate GUVs, optical tweezers to extract membrane nanotube and confocal and STED scanning for the fluorescence imaging as shown in Fig. 1 in the main text. The setup allowed us to measure the nanotube diameter at varying aspiration pressures using STED microscopy. The schematic of all the optical components of the set-up is shown in Fig. S1.

S3.1 Optical tweezers setup and calibration

The optical tweezers was built on a STED imaging system (Abberior GmbH, Germany) based on Olympus IX83 (Olympus Inc.) microscope. An expanded and collimated TEM₀₀ mode continuous wave laser beam centered at 1064 nm wavelength from a Nd:YAG laser (YLR-10-LP, IPG Photonics Corp.) was inserted from the back port of the microscope to the sample stage through a 60× water immersion objective (NA 1.2, UPLSAPO60, Olympus Inc., Japan) to form a stable optical trap. The typical laser power used for trapping was 100 mW at the sample. The bright field image of the trapped object was collected using a monochromatic CCD camera (JENOPTIK "ProgRes M") positioned at the back port of the microscope.

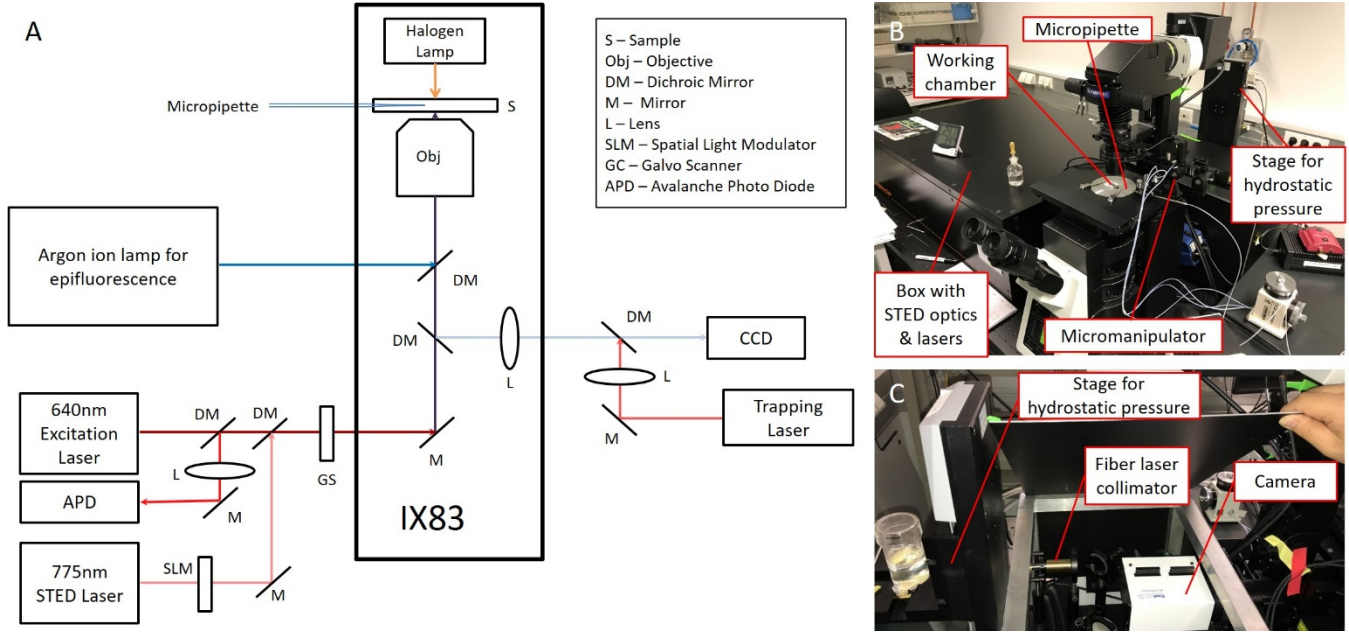


Figure S1. (A) Basic schematics of the main components of the experimental setup for STED imaging and optical trapping, and pictures of the front view (B) and the back view (C) of the actual setup with indicated components.

The trap stiffness (κ_{tr}) was calibrated using the viscous drag method, where the sample is displaced at different constant velocities (v) below the escape velocity while holding the bead with the tweezers. Using a motorized stage (BX3-SSU-1-2 motorized xy-table), the sample was displaced along the axis at which the nanotube is being pulled. The position of the trapped bead was determined using centroid tracking algorithm⁴ written in MATLAB (Mathworks Inc) where the particle position is estimated from frame-to-frame using a cross-correlation peak centroid estimation technique⁵. All measurements were performed at a height of $\sim 20 \mu\text{m}$ above the glass boundary of the sample chamber. The force on a bead with radius r exposed to drag from the surrounding medium with dynamic viscosity η is given by:

$$f_{dr} = 6\pi r\eta v \quad (S1)$$

The force F_{dr} changes the position of the trapped bead from its equilibrium position in the center of the trap, x_0 , to a newer position, x . The force on the bead due to this off-centering $\Delta x = x - x_0$ is $f_x = \kappa_{tr}\Delta x$ balances the viscous drag force. Equating f_x with f_{dr} yields the trap stiffness

$$\kappa_{tr} = 6\pi r\eta \frac{v}{\Delta x} \quad (S2)$$

which we assess from the dependence of the off-center displacement from the stage velocity, see Fig. S2. The trap stiffness was found to be $(74 \pm 2) \text{ pN}/\mu\text{m}$ at our working conditions ($r = 1 \mu\text{m}$, $\eta = 0.93 \text{ mPa}\cdot\text{s}$).

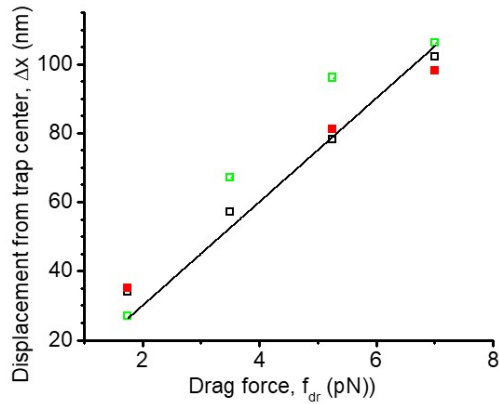


Figure S2. Plot of the viscous drag force, $f_{dr} = 6\pi\eta v$, vs. off-center displacement, Δx . Different colors correspond to different particles measured. The inverse slope of the linear fit yields the trap stiffness κ_{tr} .

The values of the trap stiffness can be used to estimate the typical fluctuation amplitude of the bead in the trap. The relation between the mean square displacement of the trapped bead (Δx^2) and κ_{tr} follows from the equipartition theorem:

$$\Delta x^2 = \frac{k_B T}{\kappa_{tr}} \quad (S3)$$

where, k_B is Boltzmann constant and T is experimental temperature. For $\kappa_{tr} = 74 \text{ pN}/\mu\text{m}$, the root mean square displacement ($\sqrt{\Delta x^2}$) is around $\sim 7.4 \text{ nm}$, inferring that the movement range of the trapped microsphere due to thermal motion is $\sim 15 \text{ nm}$ in x -axis.

S3.2 Working chamber and micropipette aspiration

Micropipettes were pulled from borosilicate capillaries (1B100-4, World Precision Instruments) using pipette puller (Sutter Instruments, Novato, CA). The tips of the prepared micropipettes were cut and shaped to desirable diameter ($3 \mu\text{m} - 5 \mu\text{m}$) using a microforge (Narishige Corp., Japan). Two coverslips of thickness $\sim 170 \mu\text{m}$ (No. 1.5) were fixed against each other separated by Π -shaped Teflon spacer to form a sample chamber of length $\sim 18 \text{ mm}$, width $\sim 15 \text{ mm}$ and height $\sim 2 \text{ mm}$. The cover glass chamber and the micropipette were coated with 1 mg/ml BSA solution to prevent the adhesion of the GUVs to them. Then they were rinsed using the external vesicle buffer (40 mM glucose and 30 mM NaCl). The sample chamber was mounted on the microscope stage. The vesicle solution diluted 20 times with isotonic experimental buffer was introduced in the sample chamber together with streptavidin-coated beads (Polyscience Inc., Cat #24160, with an average diameter of $\sim 1.9 \mu\text{m}$). The presence of NaCl salt was necessary for the strong non-covalent binding of biotin-streptavidin to pull the membrane nanotube⁶. With this combination of sugar and salt, the GUVs were able to form strong biotin-streptavidin bonds while their shapes were not deformed due to gravity. A micropipette was inserted from the open end of the sample chamber using a three dimensional water hydraulic micromanipulator system (Narishige Corp., Japan) clamped to the microscope. Zero pressure across the micropipette tip, positioned at $20 \mu\text{m}$ above the cover glass (the height of the tube-pulling experiment), was calibrated by watching the flow of streptavidin-coated particles near and inside the micropipette tip. To avoid evaporation, the water-air interface at the open side of the chamber was then covered by a drop of mineral oil. The micropipette aspiration of GUVs was controlled through a water reservoir placed on a vertical motorized linear translational stage (M-531.DD, Physik Instrumente, Germany) connected to the pipette holder. For extruding a membrane nanotube from the vesicle, a floppy GUV was held at a low aspiration pressure and brought into contact with an optically trapped streptavidin bead for few seconds. The floppiness and low aspiration tensions allow for the manipulated bead to be brought in contact with a larger fraction of the vesicle membrane (tense vesicles will allow only for point contact between the bead and vesicle) resulting in stronger adhesion as required for pulling out tubes. Then, by means of displacing the aspiration pipette mounted on a micromanipulator, the aspirated GUV was displaced away from the trapped bead by $\sim 10 \mu\text{m}$. Due to the strong biotin-streptavidin bonding, a thin membrane nanotube is formed in this process. Then the aspiration pressure was increased so that the length of the GUV tongue inside the micropipette is higher than the micropipette radius. The membrane nanotube diameter was measured by STED scanning of the extruded membrane nanotube at different aspiration pressures.

S3.3 3D STED imaging and comparison to 2D STED

To measure the diameter of the membrane nanotube, 3D STED line scan was used. The STED microscopic system (Abberior GmbH, Germany) is a commercial microscope based on an inverted microscope (IX83, Olympus Inc., Japan). The STED system contains four lasers at 405 nm, 480 nm, 561 nm and 640 nm for fluorescence excitation, allowing multicolor imaging (not employed in this work). The depletion laser is centered at 775 nm. In the path of the STED laser, a spatial light modulator (SLM) is present to generate both 2D and 3D STED beams, see Fig. S1. Both the fluorescence excitation and STED beams are focused onto the sample by the same objective which is used for the optical trapping after passing through a galvo-scanning mirror unit. Fluorescence signal generated from the sample is collected by the same objective and passed through a confocal pinhole to discard the out-of-focus signal and finally focused onto APD detectors (Fig. S1). In our experiments, the 640 nm laser was used for fluorescence excitation. As the imaging was performed 20 μm above the cover glass, a continuous auto-focus unit (ZDC2, Olympus Inc., Japan) was used. The beam profile of fluorescence excitation and 3D STED beam were measured using 150 nm gold nanoparticles (Abberior Nanoparticle Set for Expert Line 595 & 775 nm, Item number: AS-595-775-NP) as shown in Fig. S3.

The STED resolution was measured by 28 nm diameter crimson microspheres (F8782, Invitrogen) and found to be < 40 nm (Fig. S4). Thus, our STED system is capable of measuring diameter of the membrane nanotubes with radius larger than 40 nm. The 2D STED images are much brighter compared to those acquired with 3D STED at the same experimental condition, but the 2D STED images include fluorescence signal originating from out-of-focus parts of the membrane nanotube because of poor axial resolution⁷. This effectively leads to a decrease in the resolution preventing the clear detection of the two wall cross-sections of the nanotubes. This is demonstrated in Fig. S5, where the line profile across a membrane tube shows different peak heights – higher for the 2D STED image, but with resolvable peaks in 3D STED profile. The two peaks in the 3D STED line profile denote the two wall-crossings of the nanotube which cannot be detected in the 2D STED line scan where light is collected practically from the whole tube cross-section, the z-resolution being roughly 120 nm in this case. We explored pixel sizes of 5 nm, 10 nm and 20 nm when performing the line scanning and found that with decrease in the pixel size, the data contains more noise from nanotube fluctuation and has more peaks (Fig. S6). Note that scanning with smaller pixel size requires longer time lead to more vibration of the nanotube and hence noisier data. Thus, 20 nm pixel size was chosen for the experiments. Also, 20 nm pixel size is half of the STED resolution which is typical for STED scanning⁸.

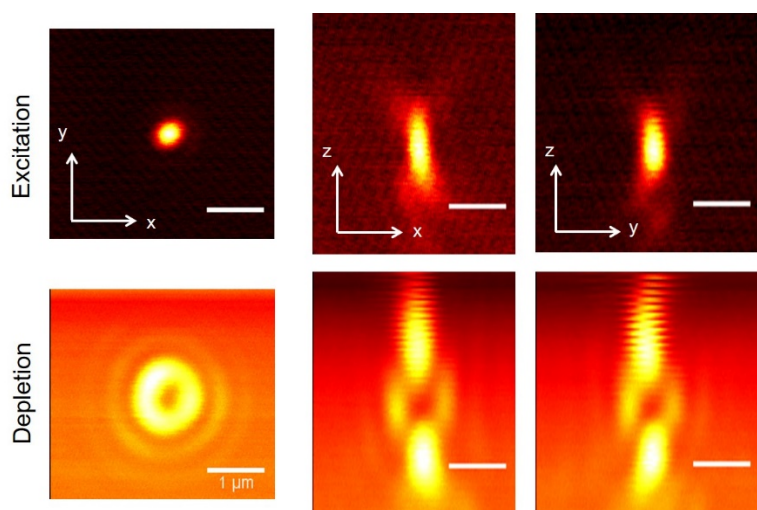


Figure S3: The beam profile of excitation laser (640 nm) (top) and 3D depletion laser (775 nm) (bottom) shown in the xy-plane (left), xz-plane (middle) and yz-plane (right). These profiles were measured using the reflection from 150 nm gold nanoparticles. Scale bars: 1 μm .

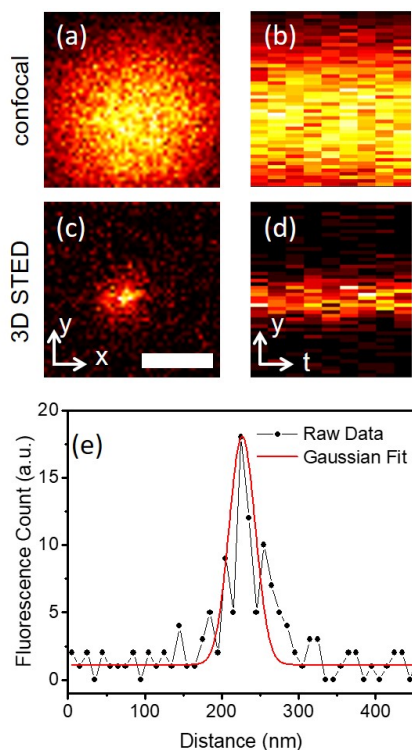


Figure S4: Confocal (a) and 3D STED (c) image of 28 nm crimson beads immobilized on a cover slip. The pixel size was set to 10 nm. The scale bar corresponds to 200 nm. Kymograph of the same crimson bead in y axis (perpendicular to membrane nanotube) for (b) confocal and (d) 3D STED scanning. Nine line scans were performed at 10 μ s pixel dwell time with 10 nm pixel size (each line scan takes 0.5 ms). (e): Gaussian fitting of the y-line scan gives 3D STED resolution to be better than 40 nm.

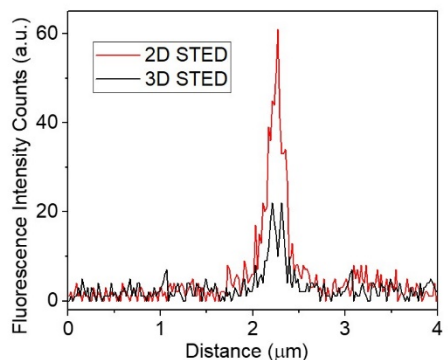


Figure S5. Intensity profile along a line scan across a membrane nanotube with 2D (red) and 3D (black) STED beams collected with pixel size of 20 nm. The 2D STED image is brighter but its effective resolution is lower due to the fluorescence signal arising from the out-of-focus part of the nanotube in z-axial direction. The signal-to-noise ratio for 3D STED is reduced but still sufficiently high (presumably because of the high quantum efficiency of the dye) to resolve the tube walls seen as peaks.

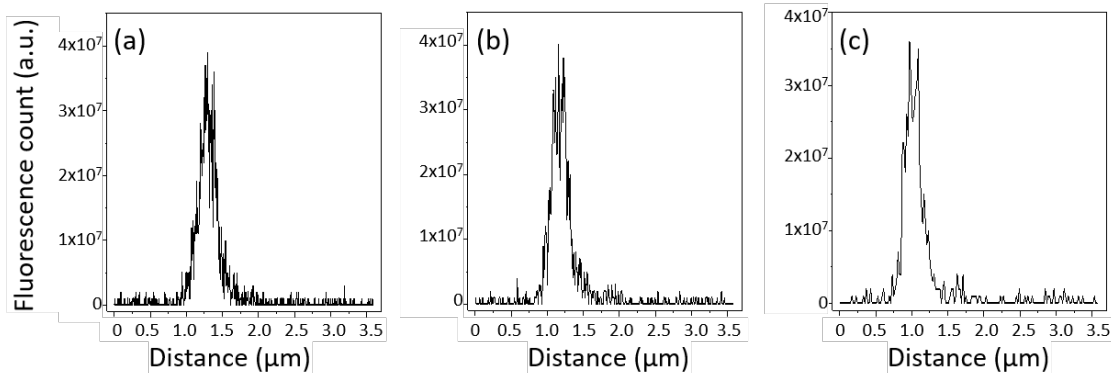


Figure S6. Line scan of a nanotube using (a) 5 nm, (b) 10 nm and (c) 20 nm pixel size. At 20 nm pixel size, the data not only becomes smoother (higher signal-to-noise ratio) but it also allows distinguishing the precise position of the two peaks indicative for the wall-crossings of the membrane nanotube.

S4 STED image analysis

To measure the tube diameter, a small image region (typically, $1 \times 1 \mu\text{m}$) including the extruded nanotube was chosen (typically in the middle of the nanotube) and 100 line scans were performed through the selected portion of the nanotube in direction perpendicular to its length (along the y-axis in Fig. 1b in the main text). The reliable and unbiased extraction of nanotube diameters was complicated by fluctuations of the nanotubes during the measurement. These fluctuations lead to a spatial displacement of the nanotube between individual scans (both in y- and z-directions, i.e. also out-of-focus), obscuring the extraction of the tube diameter. We employed an automated image analysis routine to align the individual line scans. An example of an experimentally obtained kymograph is shown in Fig. 2a in the main text. To obtain subpixel accuracy the individual line scans were linearly interpolated (interp1, MATLAB 2014a) to 0.1 pixel resolution. The individual line scans were then aligned by maximizing the overlap of the integrated intensity between two consecutive line scans l_j and l_j of length m as measured by

$$\max_{k \in \{-2m, 2m\}} \int l_{i+1}(n-k)l_i(n)dn$$

where the integral is evaluated numerically (trapz, MATLAB 2014a). The line scan l_i is shifted by the value of k at maximal overlap relative to the next line scan with $i=i+1$. By iterating over all line scans, an aligned kymograph is obtained. As judged from the confocal image, the nanotube stays on average in focus during the measurement. The aligned line scans in the kymograph were then averaged as shown in Fig. 2d in the main text and the tube diameter determined from the distance between the two major maxima corresponding to the wall-crossing of the tube. Figure S7 shows the dependence of the measured tube diameter on the applied membrane tension of the aspirated vesicle (same data as in Fig. 3 in the main text).

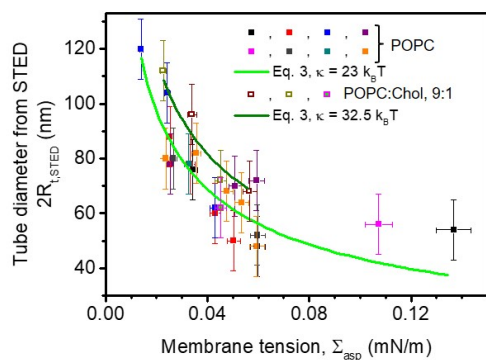


Figure S7. Plot of membrane nanotube diameter as directly measured using STED ($R_{t,STED}$) at varying membrane tension Σ_{asp} and for vesicles with two compositions – POPC (solid symbols) and POPC:Chol 9:1 (open symbols). Different colors correspond to measurements on different vesicles. The two curves show the calculated tube diameter using Eq. 3 in the main text with bending rigidity $\kappa = 23 k_B T$ as measured independently for POPC membranes, and $\kappa = 32.5 k_B T$ as assessed from literature values for membranes made of POPC:Chol 9:1.

S5 Tube pulling experiment for deducing the membrane bending rigidity

Pulling of outward membrane nanotubes from GUVs can be used to assess the membrane bending rigidity. For symmetric membranes, the pulling force is $f_t = 2\pi\sqrt{2\kappa\Sigma_{asp}} - 4\pi\kappa m - \pi\kappa/R_v$ (see main text for notations). Thus, the bending rigidity κ can be directly obtained from the slope of the dependence of the pulling force, f_t , vs. $\sqrt{\Sigma_{asp}}$ (Fig. S8). For this experiment, the trap force was measured from the displacement of the bead away from the trap center, Δx . Bright field images of the trapped bead were collected using the CCD camera at the back port of the microscope. The bead was first recorded free and then attached via a nanotube to the GUV held by a micropipette at different aspiration pressures. For each of these measurements, 100 frames were collected with 1 ms exposure time at 9 frames per second. As explained in Section S3.1, the sub-pixels bead position was determined using centroid tracking algorithm⁴. The trap force was then determined from $f_t = \kappa_{tr} \Delta x$ using the predetermined trap constant κ_{tr} .

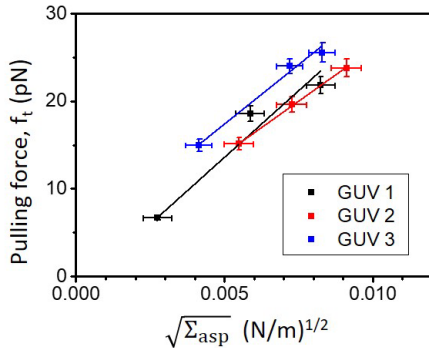


Figure S8. Pulling force versus the square root of membrane tension (Σ_{asp}) for three different GUVs. The solid lines are the linear fit for the data of the respective GUVs. The bending rigidity is found to be $\kappa = 23 \pm 5$ k_BT.

Movie S1. Example for a fluctuating floppy vesicle suitable for micropipette aspiration (real time, 10 s at 24 frames per second). The scale bar corresponds to 10 μ m.

References

1. Angelova, M. I.; Dimitrov, D. S., Liposome Electroformation. *Faraday Discussions* **1986**, *81*, 303-311.
2. Dimova, R., Giant Vesicles and Their Use in Assays for Assessing Membrane Phase State, Curvature, Mechanics, and Electrical Properties. *Annu. Rev. Biophys.* **2019**, *48* (1), 93-119.
3. Gracià, R. S.; Bezlyepkina, N.; Knorr, R. L.; Lipowsky, R.; Dimova, R., Effect of cholesterol on the rigidity of saturated and unsaturated membranes: fluctuation and electrodeformation analysis of giant vesicles. *Soft Matter* **2010**, *6* (7), 1472-1482.
4. Dasgupta, R.; Verma, R. S.; Gupta, P. K., Microfluidic sorting with blinking optical traps. *Opt. Lett.* **2012**, *37* (10), 1739-1741.
5. Gelles, J.; Schnapp, B. J.; Sheetz, M. P., Tracking kinesin-driven movements with nanometre-scale precision. *Nature* **1988**, *331* (6155), 450-453.
6. Prévost, C.; Tsai, F.-C.; Bassereau, P.; Simunovic, M., Pulling Membrane Nanotubes from Giant Unilamellar Vesicles. *JoVE* **2017**, (130), e56086.
7. Sahl, S. J.; Hell, S. W.; Jakobs, S., Fluorescence nanoscopy in cell biology. *Nat. Rev. Mol. Cell Biol.* **2017**, *18*, 685.
8. Lauterbach, M. A.; Keller, J.; Schönle, A.; Kamin, D.; Westphal, V.; Rizzoli, S. O.; Hell, S. W., Comparing video-rate STED nanoscopy and confocal microscopy of living neurons. *Journal of Biophotonics* **2010**, *3* (7), 417-424.